THE ASTROPHYSICAL JOURNAL, 460:L61–L64, 1996 March 20

HIGH-RESOLUTION OBSERVATIONS OF INTERSTELLAR C_2 TOWARD ζ OPHIUCHI

KENNETH R. SEMBACH,[1,2] ANTHONY C. DANKS,[1,3] AND DAVID L. LAMBERT[4]
Received 1995 November 22; accepted 1996 January 8

ABSTRACT

We present high-resolution ($\lambda/\Delta\lambda \approx 540{,}000$) absorption-line observations of two weak C_2 lines in the 2–0 band of the Phillips system in the direction of ζ Ophiuchi. These high signal-to-noise ratio (S/N ≈ 230–380) data were obtained at the McDonald Observatory 2.7 m telescope using the coudé echelle spectrograph in double-pass mode. The C_2 line profiles are resolved into two components, having a spacing of ≈1.14 km s^{-1}, as has been seen for other molecular species such as CN, CO, and CH. Unlike these molecules, however, the strengths of the two narrow C_2 components are very similar. We briefly discuss the implications these results have for understanding the chemical behavior of diatomic molecules in diffuse interstellar clouds.

Subject headings: ISM: molecules — line: profiles — stars: individual (ζ Ophiuchi)

1. INTRODUCTION

Interstellar C_2 toward ζ Ophiuchi was discovered by Chaffee & Lutz (1978), who detected a single line of the 2–0 band of the Phillips system. Subsequent observations of this band near 8760 Å (Hobbs & Campbell 1982; Danks & Lambert 1983) and of the 3–0 band near 7720 Å (van Dishoeck & Black 1986) have led to detections of many additional lines; the relative populations of the ground-state rotational ladder are now known for the even levels between $J = 0$ and $J = 14$. (Odd J levels do not exist for homonuclear molecules with zero-spin nuclei.) Examination of the rotational ladder has been extended to $J = 24$ through *Hubble Space Telescope* (*HST*) observations of the 0–0 band of the Mulliken system (Lambert, Sheffer, & Federman 1995). None of these observations, however, have resolved the C_2 line profiles.

High spectral resolution observations of other interstellar molecular absorption lines toward ζ Oph—CN at 3875 Å, CH at 4300 Å, and CH^+ at 4232 Å—show that two to three distinct components may be hidden within an unresolved line (Lambert, Sheffer, & Crane 1990; Crawford et al. 1994). In particular, the CN lines consist of two narrow components of unequal strength and line width separated by 1.2 km s^{-1}. Observations of the CH 9 cm radio emission line (Liszt 1979; Willson 1981) and CO emission (Crutcher & Federman 1987; Le Bourlot, Gerin, & Perault 1989; Liszt 1993, 1994) at millimeter wavelengths in the pure rotation lines $J = 1–0$ and 2–1 also show two narrow components with a separation of 1.2 km s^{-1}. CH^+ exhibits only a single broad line, and CH has a composite profile consisting of two narrow components (CN-like) and a broad component (CH^+-like). The different profile shapes provide important clues to the formation of these molecules. For this reason, we observed two C_2 lines from the 2–0 band of the Phillips system. Our new high-resolution spectra clearly show that C_2 has two sharp components of nearly equal strength separated by 1.14 km s^{-1}. We comment briefly on the significance of this result for chemical schemes designed to explain the formation/destruction of various diatomic molecules in diffuse clouds.

[1] Guest Observer, McDonald Observatory.
[2] Center for Space Research, Massachusetts Institute of Technology, Cambridge, MA 02139.
[3] STX Systems, Goddard Space Flight Center, Greenbelt, MD 20771.
[4] Department of Astronomy, University of Texas, Austin, TX 78712.

2. OBSERVATIONS

We obtained observations of the 2–0 Phillips C_2 $Q(2)$ and $Q(4)$ absorption lines in the spectrum of ζ Oph using the McDonald Observatory 2.7 m telescope on 1994 June 24 and 25. The coudé spectrograph was used in double-pass mode (Tull 1972), with an advanced imaging system (AIS) camera mounted at the focus of the spectrograph. The AIS system has a 2048^2 pixel front-side–illuminated Scientific Imaging Technologies CCD, with a lumigen overcoat. The CCD has 21 μm pixels, and is a prototype for the detectors to be used in the Space Telescope Imaging Spectrograph (STIS). Two-pixel on-chip binning in the dispersion direction was used, since the line profiles were significantly oversampled. Approximately 5.8 Å of spectrum was recorded for each line, and of this total wavelength coverage approximately 3.1 Å was unvignetted by the spectrograph optics. The C_2 lines were placed in the unvignetted portion of the beam, and several series of exposures were obtained at different locations on the CCD to optimize the S/N ratio of the combined spectra.

We removed the bias level, subtracted the background light, and flat-fielded each observation with the dispersed spectrum of a quartz lamp, which illuminated the spectrograph slit. The stellar spectra in the images were traced, extracted, and co-added using standard single-order reduction procedures (Sembach, Danks, & Savage 1993). Cosmic rays were removed during the extraction procedure by an iterative algorithm that searches for deviant upward noise spikes.

Wavelength calibration was achieved for the C_2 $Q(2)$ line at 8761.188 Å by obtaining an 1800 s Th-Ar lamp exposure immediately prior to the observations. The wavelength solution, determined by a linear fit to the three arc lines in the spectrum (8758.2434 [Th], 8760.4496 [Th], and 8761.6862 [Ar] Å; Willmarth 1987), has a velocity uncertainty (1 σ) of ≈0.08 km s^{-1}. The calibration for the $Q(4)$ line at 8763.753 Å, which lies in a spectral region with no nearby arc lines, was made by noting the pixel location of (1) a weak Fe I line (8763.978 Å; Moore, Minnaert, & Houtgast 1966) in a solar spectrum obtained by observing the day sky at the same grating location and (2) the C_2 $Q(2)$ line in the vignetted portion of the spectrum. The dispersion per pixel was found to be the same as that for the $Q(2)$ line, ≈5.86 mÅ pixel^{-1}. An upper limit to the velocity resolution of the spectra obtained from the measured FWHM of the Th-Ar lines in the $Q(2)$

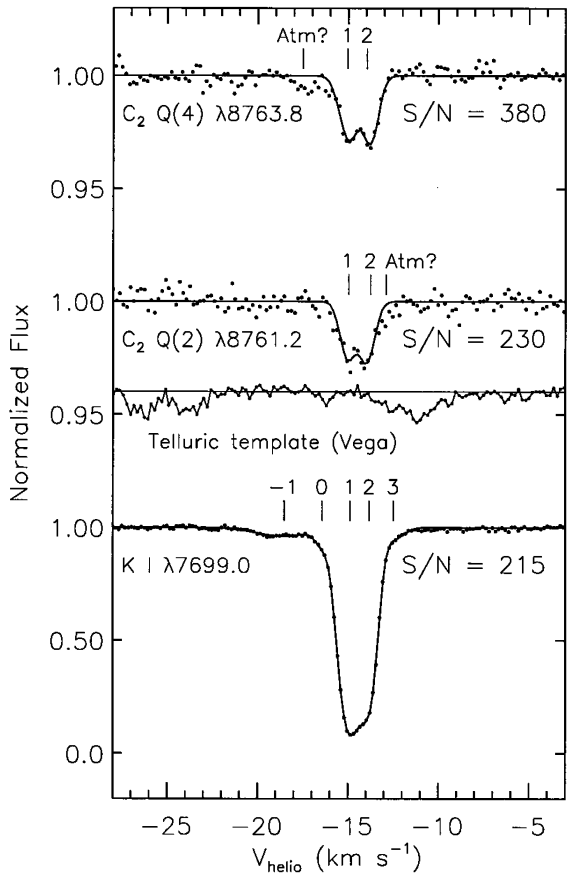

FIG. 1.—Continuum-normalized absorption profiles of C_2 $Q(4)$, C_2 $Q(2)$, and K I toward ζ Oph. The data (*circles*) have a resolution of ≈0.56 km s^{-1}. The best-fit profiles (*smooth lines*) are characterized in Tables 2 and 3. Note the double-component nature of the profiles. The telluric template for Vega is inset under the C_2 $Q(2)$ profile.

spectral region is ≈0.8 km s^{-1} (≈4 pixels after binning) for the 120 μm slit used for all observations. Since the intrinsic widths of the Th-Ar lines contribute to the line width measurement (≈0.55 km s^{-1} for Th; see Welty, Hobbs, & Kulkarni 1994), the actual resolution achieved is probably much closer to the value of 0.56 km s^{-1} expected from the projected slit width. We adopt the latter value in our analysis.

For comparison with the molecular data, we observed the K I line at a wavelength of 7698.974 Å. The K I line traces absorption in dense *atomic* gas along the sight line. We also obtained spectra of Vega at the C_2 $Q(2)$ and K I setups to use as templates for removal of very weak telluric lines arising in the Earth's atmosphere (see Fig. 1).

3. MEASUREMENTS

We present integrated equivalent widths and column densities for the C_2 and K I lines in Table 1. All errors are 1 σ estimates unless otherwise specified. Exposure times and final S/N ratios are also listed. The continuum fitting and error estimation procedures are similar to those described by Sembach & Savage (1992). The continuum normalized line profiles are shown in Figure 1. The shallow absorption near −17.5 km s^{-1} in the $Q(4)$ spectrum is probably a weak telluric line, since it does not appear in either the $Q(2)$ or the K I line profiles. Note the clear evidence for two components in both C_2 lines,

TABLE 1

EQUIVALENT WIDTHS AND COLUMN DENSITIES

Species	λ_{air} (Å)	S/N	Exposure Time (minutes)	W_λ (mÅ)	N (10^{12} cm^{-2})
K I	7698.974	215	210	62.7 ± 0.5	>0.35
C_2 $Q(2)$	8761.188	230	210	1.9 ± 0.2	3.87 ± 0.41
C_2 $Q(4)$	8763.753	380	270	2.0 ± 0.1	4.07 ± 0.20

as well as the asymmetric character of the K I line, which suggests that at least two atomic gas components are present at velocities near those of the molecular lines. Examples of high-resolution interstellar Na I, Ca II, and Fe I profiles for the sight line can be found in Welty et al. (1994) and Barlow et al. (1995).[5]

The C_2 equivalent widths in Table 1 are slightly different from those found in previous studies of the ζ Oph sight line. Our values of 1.9 ± 0.2 mÅ for $Q(2)$ and 2.0 ± 0.1 mÅ for $Q(4)$ are larger than the values of 1.2 and 1.5 mÅ obtained by Hobbs & Campbell (1982), or the values of 1.2 and 1.7 mÅ found by Danks & Lambert (1983). However, the values agree to within the 2 σ errors of the measurements. An earlier measurement of $W_{\lambda,Q(2)}$ = 2.1 ± 0.2 mÅ (Chaffee & Lutz 1978) agrees well with our integrated measurement. There may still be some weak telluric absorption, of order 0.2–0.4 mÅ, in the C_2 lines that we have not accounted for in our reduction. The feature near the $Q(4)$ line, for example, has $W_\lambda \sim 0.3$ mÅ. Our total K I equivalent width of 62.7 ± 0.5 mÅ agrees well with prior measurements of 62 ± 1 mÅ (van Dishoeck & Black 1986) and 63 mÅ (Lemoine, Ferlet, & Vidal-Madjar 1995).

In Tables 2 and 3 we list the results derived by fitting the C_2 and K I lines with multiple Gaussian components. The fitting procedure was similar to that described by Sembach et al.

[5] Inspection of our K I line centroid with that found by Lemoine et al. (1995) in their $\lambda/\Delta\lambda \approx 10^5$ spectrum from the European Southern Observatory, as well as the very high resolution Na I and Ca II spectra published by Barlow et al. (1995), indicated that our K I spectrum needed to be shifted by ≈+0.3 km s^{-1}. Since our wavelength calibration of the K I line was based on atmospheric and solar absorption lines (see Moore et al. 1966), we adopt this additional velocity shift throughout for consistency with published work.

TABLE 2

C_2 PROFILE FIT RESULTS

Species	Component Number	$\langle v_{helio} \rangle$ (km s^{-1})	b (km s^{-1})	$N(J)$ (10^{12} cm^{-2})
$Q(2)$	1	−15.03 ± 0.12	0.48 ± 0.18	1.56 ± 0.44
$Q(4)$	1	−14.96 ± 0.12	0.61 ± 0.10	2.18 ± 0.31
$Q(2)$	2	−13.96 ± 0.11	0.51 ± 0.23	1.75 ± 0.40
$Q(4)$	2	−13.76 ± 0.10	0.47 ± 0.10	1.86 ± 0.34

TABLE 3

K I PROFILE FIT RESULTS

Component Number	$\langle v_{helio} \rangle$ (km s^{-1})	b (km s^{-1})	N (10^{11} cm^{-2})
−1.....	−18.53 ± 0.26	2.11 ± 0.17	0.22 ± 0.02
0.....	−16.41 ± 0.06	0.41 ± 0.06	0.09 ± 0.02
1.....	−14.87 ± 0.04	0.64 ± 0.05	4.69 ± 0.10
2.....	−13.81 ± 0.05	0.47 ± 0.05	2.31 ± 0.07
3.....	−12.48 ± 0.11	0.69 ± 0.11	0.10 ± 0.02

TABLE 4

COMPARISON OF C_2, CN, AND CH PROFILES

	Component 1		Component 2		
Molecule	$\langle v_{helio} \rangle$ (km s^{-1})	b (km s^{-1})	$\langle v_{helio} \rangle$ (km s^{-1})	b (km s^{-1})	$N(2)/N(1)$
C_2	-15.00 ± 0.08	0.54 ± 0.10	-13.86 ± 0.07	0.49 ± 0.13	0.99 ± 0.23
CN[a]	-15.08 ± 0.05	$0.55^{+0.05}_{-0.10}$	-13.92 ± 0.05	0.45 ± 0.10	0.40 ± 0.1
CH[b]	-14.70 ± 0.05	$0.58^{+0.05}_{-0.13}$	-13.60 ± 0.05	$0.50^{+0.50}_{-0.20}$	0.45 ± 0.1

[a] CN $R(0)$ line (Crawford et al. 1994).
[b] CH $R(1)$ line (Crawford et al. 1994). This line also has a broader ($b \approx 1.8$ km s^{-1}) component.

(1993). The fits are shown as smooth lines in Figure 1. Estimates of the relative populations of the C_2 $J'' = 2$ and $J'' = 4$ lines in the Mulliken band observed with the Goddard High Resolution Spectrograph (GHRS) (Lambert et al. 1995) yield $N(J'' = 4)/N(J'' = 2) = 1.13 \pm 0.11$, in good agreement with our measured value of 1.05 ± 0.12 (Table 1) or component fitting value of 0.97 ± 0.20 (Table 2). The total value of $N(\text{K I}) = 7.4 \times 10^{11}$ cm^{-2}, found from the component fitting, is consistent with a curve-of-growth analysis that includes the weak line equivalent widths [$W_\lambda(4044$ Å$) = 0.8$ mÅ, $W_\lambda(4047$ Å$) = 0.3$ mÅ] found by Shulman, Bortolot, & Thaddeus (1974).

4. RESULTS AND INTERPRETATION

Observations of radio-millimeter CH and CO emission lines and recent high-resolution observations of optical CN and CH absorption lines show that these lines are resolvable into two components separated by 1.2 km s^{-1}. Therefore, it has been supposed that the sight line samples two clouds or clumps of gas. The CH^+ ion produces a distinctly broader optical line that has a counterpart in the optical CH line but not in the CN optical line or the CO and CH emission lines. As a first step in the interpretation of our results for the C_2 lines, we compare the line parameters with those of the two CN and CH components, as measured by Crawford et al. (1994). Table 4 lists heliocentric velocities, line widths expressed by the customary b-value,[6] and ratios of the column densities in the two components.

The C_2 molecules are clearly present in both of the clouds revealed by the CH, CN, and CO observations. In particular, the separation between the C_2 components is 1.14 ± 0.11 km s^{-1}. This separation is in excellent agreement with that measured from the CO emission lines (1.18 ± 0.02 km s^{-1}; Le Bourlot et al. 1989) and, more significantly, with that derived from the optical CN line (1.18 ± 0.06 km s^{-1}, Lambert et al. 1990; 1.16 ± 0.07 km s^{-1}, Crawford et al. 1994).

Heliocentric velocity determinations for the C_2 lines are compromised slightly by the paucity of reference lines in the Th-Ar spectrum or of telluric lines in the stellar spectrum (see above). The absolute wavelengths of the C_2 lines, however, are well determined. Chauville, Maillard, & Mantz (1977), who recorded the spectrum of an acetylene flame in oxygen, give vacuum frequencies for the $Q(2)$ and $Q(4)$ lines. On conversion to wavelengths in standard air, the $Q(2)$ line is at 8761.194 Å and the $Q(4)$ line is at 8763.750 Å, with an uncertainty of $\approx \pm 0.005$ Å (0.2 km s^{-1}). Douay, Nietmann, & Bernath (1988) observed several infrared bands of the Phillips system and derived a new set of molecular constants. Although the 2–0 band was not observed, Douay et al. remark that their molecular constants should give wavelengths for the 2–0 band that are more accurate than published values. These constants yield wavelengths of 8761.188 and 8763.753 Å for the $Q(2)$ and $Q(4)$ lines, respectively, with uncertainties of less than 1 mÅ. These predictions, which are consistent with the measurements of Chauville et al., are adopted here. (Accurate rest wavelengths for the CN and CH lines tabulated by Black & van Dishoeck 1988 and adopted by Crawford et al. 1994 are not a significant source of uncertainty in our velocity comparisons.) The C_2 component velocities listed in Table 4 are in very good agreement with those for CN, but differ slightly from those for CH. The CN and CH line centroid differences appear to be real (see Lambert et al. 1990).

The b-values of the CN and CH lines listed in Table 4 agree very well. Results for the CN line are the more precise because the CH line profile also receives a substantial contribution from a broad ($b = 1.8$ km s^{-1}; Crawford et al. 1994) component. The results of Lambert et al. (1990) for the CN line are quite similar to those in Table 4: $b = 0.59 \pm 0.04$ and 0.38 ± 0.08 km s^{-1} for components 1 and 2, respectively. The agreement between the two studies is slightly less satisfactory for the CH components; Lambert et al. obtained $b = 0.75 \pm 0.02$ and 0.44 ± 0.08 km s^{-1}. The C_2 lines have b-values that are consistent with those of the CN and CH lines. If a larger instrumental width is adopted in the fitting process, these b-values will decrease; the b-value of component 2 could be as much as a factor of 1.5 lower if we adopt an instrumental width of 0.8 km s^{-1}.

A marked disagreement for the width of the broad CH component is found between the two published analyses ($b = 3.1 \pm 0.2$ vs. $b = 1.8 \pm 0.5$ km s^{-1}), which is probably an indication that the width used for the broad component is still somewhat subjective. Lambert et al. (1990) fitted the CH^+ profile with a single broad ($b = 2.1 \pm 0.2$ km s^{-1}) Gaussian component. Gas responsible for the broad CH and CH^+ components may be considered as a third cloud, clump, or region containing very little CN or C_2. We find that less than 10% of the total column density of the C_2 lines could exist within an additional broad component with $b \approx 3$ km s^{-1}. Note that Crawford et al. (1994) assign 40% of the total CH to the broad component.

C_2 column densities are derived from the equivalent widths using an ab initio prediction of the band oscillator strength: $f_{20} = 1.44 \times 10^{-3}$ (Langhoff et al. 1990), with an estimated uncertainty of $\approx 5\%$. The f-values we adopt, $f = 7.22 \times 10^{-4}$, for the $Q(2)$ and $Q(4)$ lines are obtained from f_{20}. Our derived column densities for C_2 are about 30% higher than those obtained from the Mulliken system (Lambert et al. 1995). The combined errors of the measured equivalent widths and the f-values of the Mulliken and Phillips systems may not fully

[6] FWHM = 1.665b for a weak line.

account for this discrepancy (see Lambert et al. 1995 for a discussion of the f-values).

Fortunately, the uncertainty in the C_2 column densities is not a major contributor to the most prominent aspect of the resolved C_2 profiles—the two-component nature of the absorption. The most striking difference in Table 4 between C_2 and the other two molecules is in the *relative* strengths of the two components. For CN and CH the column density of the "red" component is ≈40% that of the "blue" component [see $N(2)/N(1)$ in Table 4], but for C_2 the two components have similar column densities.[7] In other words, the CN/C_2 ratios for the two components differ by about a factor of 2. For ^{12}CO, the red to blue component equivalent width ratio derived from emission profiles for the 1–0 and 2–1 lines from a 8 × 8 point map about ζ Oph is ≈0.6 (Le Bourlot et al. 1989), and therefore the CO/C_2 ratio varies by less than the CN/C_2 ratio between the two components.

The difference in relative column densities between C_2 and CN (and CH) is a clue to the physical conditions in the two clouds. In a survey of C_2 and CN in 33 diffuse cloud lines of sight, Federman et al. (1994) found a strong correlation between their column densities—the slope of the relation between log N(CN) and log $N(C_2)$ was 1.56 ± 0.09 with a correlation coefficient of 0.85. When ζ Oph is represented by its total CN and C_2 column densities, it falls very close to the Federman et al. relation. Component 2 falls on the relation, but at the lower end of its defined range and just beyond the points with the lowest measured column densities of CN and C_2. The sight line toward ξ Per is the only one with a lower measured column density of C_2 (Lambert et al. 1995). Component 1 falls above the relation (too much CN for the given amount of C_2), but not by an unusually large amount. (It should be noted that all of the points defining the relation were obtained from unresolved line profiles tracing two or more clouds along most lines of sight.)

Federman et al. (1994; see also Federman & Lambert 1988) discuss the synthesis of CN and C_2 in diffuse clouds using a reaction network linking these molecules to CH. Formation of C_2 proceeds from CH, while formation of CN occurs through two channels—one from C_2 and the other from CH. The molecular densities are sensitive to the ratio of the photodissociation rate to the local total density. Over a range of density, temperature, and radiation fields expected to be appropriate for diffuse and translucent clouds, CN and C_2 column densities for an observed CH column density are generally predicted correctly to within 25%. For model clouds and the adopted reaction network, the CN column density varies more steeply than the C_2 column density with the prevailing CH column density (see, especially, Figs. 2 and 3 of Federman & Lambert 1988). When the two channels are of comparable efficiency, the CN density is more sensitive to the photodissociation rates than the C_2 density. Since CH has a larger column density in component 1 than in component 2, we would expect the ratio of the CN column densities between the two components to be more severe than for C_2 as is observed. In this picture, component 2 (the "red" cloud) may experience the more intense radiation field and is possibly closer to ζ Oph.

Further insight into physical conditions and the radiation field might be obtained by observing C_2 lines from more excited rotational levels; van Dishoeck & Black (1982) show that the populations of these levels are greatly influenced by the ambient (infrared) radiation field. Determination of the line profiles for additional levels is left for a future observing run. Augmentation of the list of molecular lines for which the components are resolved would also be of great value. Carbon monoxide is an obvious case in point. Unfortunately, there is little prospect that suitable ultraviolet spectra will be available in the near future. However, CO is detectable through infrared vibration-rotation transitions, and ultra–high-resolution infrared spectrometers could be built at reasonable cost. Then, translucent and the more extreme diffuse clouds will be detectable in CO; Black & van Dishoeck (1988) show a predicted profile for the strongest infrared CO line in the ζ Oph spectrum.

We thank Bruce Woodgate and the STIS team for making the AIS camera available, and David Doss for help in setting up the instrumentation at the observatory. We thank Steve Federman for discussions concerning § 4. Dan Welty provided many useful comments that improved the manuscript.

[7] It is unlikely that any telluric absorption in the C_2 profiles would conspire in a way to make the component strengths similar in *both* lines.

REFERENCES

Barlow, M. J., et al. 1995, MNRAS, 272, 333
Black, J. H., & van Dishoeck, E. F. 1988, ApJ, 331, 986
Chaffee, F. H., Jr., & Lutz, B. L. 1978, ApJ, 221, L91
Chauville, J., Maillard, J. P., & Mantz, A. W. 1977, J. Mol. Spectrosc., 68, 399
Crawford, I. A., Barlow, M. J., Diego, F., & Spyromilio, J. 1994, MNRAS, 266, 903
Crutcher, R. M., & Federman, S. R. 1987, ApJ, 316, L71
Danks, A. C., & Lambert, D. L. 1983, A&A, 124, 188
Douay, M., Nietmann, R., & Bernath, P. F. 1988, J. Mol. Spectrosc., 131, 250
Federman, S. R., & Lambert, D. L. 1988, ApJ, 328, 777
Federman, S. R., Strom, C. J., Lambert, D. L., Cardelli, J. A., Smith, V. V., & Joseph, C. L. 1994, ApJ, 424, 772
Hobbs, L. M., & Campbell, B. 1982, ApJ, 254, 108
Lambert, D. L., Sheffer, Y., & Crane, P. 1990, ApJ, 359, L19
Lambert, D. L., Sheffer, Y., & Federman, S. R. 1995, ApJ, 438, 740
Langhoff, S. R., Bauschlicher, C. W., Jr., Rendell, A. P., & Komornicki, A. 1990, J. Chem. Phys., 92, 300
Le Bourlot, J., Gerin, M., & Perault, M. 1989, A&A, 219, 279
Lemoine, M., Ferlet, R., & Vidal-Madjar, A. 1995, A&A, 298, 879
Liszt, H. S. 1979, ApJ, 233, L147
———. 1993, ApJ, 414, 242
———. 1994, ApJ, 424, 510
Moore, C. E., Minnaert, M. G. J., & Houtgast, J. 1966, The Solar Spectrum 2935 Å to 8770 Å: Second Revision of Rowland's Preliminary Table of Solar Spectrum Wavelengths (NBS Monog. 61; Washington, DC: NBS)
Sembach, K. R., Danks, A. C., & Savage, B. D. 1993, A&AS, 100, 107
Sembach, K. R., & Savage, B. D. 1992, ApJS, 83, 147
Shulman, S., Bortolot, V. J., & Thaddeus, P. 1974, ApJ, 193, 97
Tull, R. G. 1972, in Proc. ESO/CERN Conf. on Auxiliary Instrumentation for Large Telescopes (Geneva: ESO), 259
van Dishoeck, E. F., & Black, J. H. 1986, ApJ, 307, 332
Welty, D. E., Hobbs, L. M., & Kulkarni, V. P. 1994, ApJ, 436, 152
Willmarth, D. 1987, A CCD Atlas of Comparison Spectra: Thorium-Argon Hollow Cathode 3180–9540 Å (Tucson: KPNO)
Willson, R. F. 1981, ApJ, 247, 116